must be lower. Thus, the stress appearing in high-speed heating of the blooms cannot lead to loss of continuity of the metal and hence there is a possibility of increasing the design productivity of the apparatus.

NOTATION

T, temperature; ρ, c, λ, thermophysical coefficients; α, σ, external heat-transfer coefficients; τ, time; R, characteristic dimension; σ, thermal stress in ingot cross section; ε, deformation; Δu, Δv, increments in displacements over the x, y axes; $k_\sigma = (\sigma_i - \sigma_T(T))/\sigma_T(T)$, stress-state coefficient.

LITERATURE CITED

1. T. A. Birger, and B. F. Shorr (eds.), Thermostability of Machine Parts [in Russian], Moscow (1975).
2. A. A. Poznyak, Thermodynamic Phenomena in the Crystallization of Metals [in Russian], Novosibirsk (1982), pp. 108-119.

MODELING MACROSEGREGATION IN AN INGOT, TAKING ACCOUNT OF ALLOY SHRINKAGE

L. V. Shaton, V. N. Kramarenko, and Yu. A. Samoilovich

UDC 621.746.628.011.001.573

A mathematical model is proposed for the description of zonal segregation in an ingot of quiescent steel on casting in a mold, taking account of alloy shrinkage.

Despite the development of continuous-casting technology, most the steel forged in the USSR is cast in a mold. Both technologies have a common deficiency: the larger the ingot, the more impurity segregation occurs on solidification. The mechanism of zonal-segregation formation was described in [1-4], and experimental data have been obtained on the zonal segregation of various chemical elements on casting. However, in our view, no sufficiently complete method of calculating solidification [5, 3], taking account of melt flows and maintenance of the liquid core of the ingot on alloy shrinkage [1, 2], exists as yet. A mathematical model is created in the present work for the complex investigation of these processes. It is developed for the calculation of the thermal and concentrational fields and consists of a system of differential equations with the corresponding boundary conditions.

The liquid-phase motion in the solidifying ingot is a superposition of the flux due to large-scale processes (such as stratification, mixing, etc.) and microfluxes arising on filling of the shrinkage volumes. First of all, the shrinkage component of the liquid-phase velocity is isolated, by writing the continuity equation. The metal density is a superposition of the densities of the solid ρ_s and liquid ρ_ℓ phases, which are not equal but constants: $\rho = \rho_s\varphi + \rho_\ell(1-\varphi)$.

Using the mixing rates of the solid and liquid phases v_{sh} and $v_{\ell h}$, which satisfy the incompressibility equation, and also the shrinkage component of the liquid-phase velocity $v_{\ell y}$, the continuity equation is written in the form

$$\rho_s \nabla (v_{sh}\varphi) + \rho_l \nabla (v_{lh}(1-\varphi)) = 0, \tag{1}$$

and, taking into account that $d\rho/d\tau = 0$, it follows that

$$\frac{\partial(\rho_s\varphi)}{\partial\tau} + \rho_s\nabla(v_{sh}\varphi) + \frac{\partial(\rho_l(1-\varphi))}{\partial\tau} + \rho_l\nabla[v_{lh}(1-\varphi) + v_{ly}(1-\varphi)] = 0. \tag{2}$$

Hence, substituting Eq. (1) in Eq. (2), an equation determining the shrinkage rate $v_{\ell y}$ may be obtained

$$(\rho_s - \rho_l)\frac{\partial\varphi}{\partial\tau} + \rho_l\nabla[v_{ly}(1-\varphi)] = 0. \tag{3}$$

Belorussian Polytechnical Institute, Minsk. Translated from Inzhenerno-Fizicheskii Zhurnal, Vol. 58, No. 3, pp. 405-411, March, 1990. Original article submitted June 22, 1988.

0022-0841/90/5803-0292$12.50

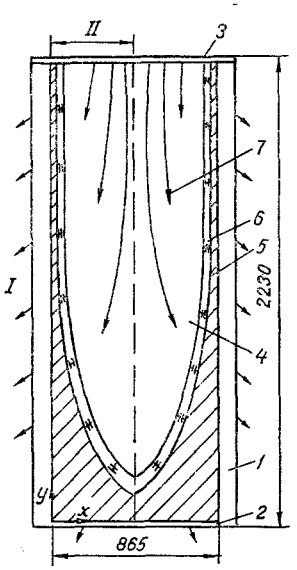

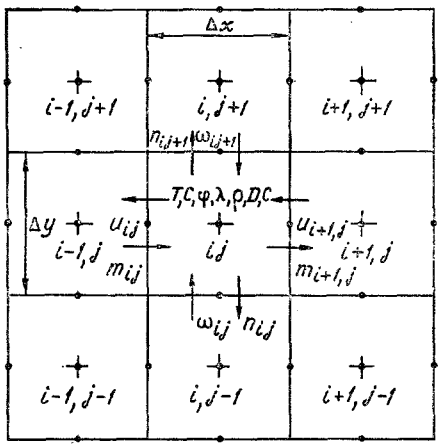

Fig. 1. Diagram of calculation region: I) heat release to the surrounding space; II) calculation region.

Fig. 2. General structure of calculation grid.

Separation of the liquid-phase velocity into two components is convenient for the subsequent analysis of the problems, where motion of the ingot as a whole and electromagnetic mixing of the liquid phase together with shrinkage filtration are present. The filtrational component may be calculated using only Eq. (3), neglecting the first two processes in the first approximation. The solution of Eq. (2) is not unique, and therefore additional assumptions must be used to obtain the specific structures of filtrational flow: for example, that the rate of filtrational flow satisfies Darcy's law [5]

$$v_{ly} = -k/(\eta(1-\varphi))(\nabla P + \rho q), \tag{4}$$

where P is the pressure in the ingot; ρq is its "gravitational" component; k is the specific permeability of the medium; η is the dynamic viscosity of the interdendritic liquid. Using Eqs. (4) and (3) leads to the need to solve an elliptical equation for the pressure and then to differentiate the solution in order to find $v_{\ell y}$. The model described below is constructed on the basis of simpler assumptions:

a) the direction of the filtrational velocity component coincides with the direction of the temperature gradient;

b) the pressure gradient is proportional to the gradient of the proportion of solid phase.

Thus, the filtration rate is determined by the gradient of the proportion of solid phase

$$v_{ly} = -\gamma\nabla\varphi, \tag{5}$$

where the coefficient γ is calculated separately for each calculational cell, so as to satisfy Eq. (3). This ensures a predominant direction of filtration from the "more liquid" metal to the "more solid" metal. In calculating the filtration-rate field, all the calculation cells are sorted in order of decreasing proportion of solid-phase. Thus, for successive cells, beginning with the first, the components of the filtration rate $v_{\ell y}$ are found using the finite-difference analog of Eqs. (3) and (5). The velocities $v_{\ell h}$, v_{sh} are assumed to be zero, but may be calculated using the Navier—Stokes equation. After calculating $v_{\ell h}$, v_{sh}, $v_{\ell y}$, the conservation equation for the enthalpy may be written, taking account of convection and heat conduction

$$\frac{dI}{d\tau} = -\nabla j, \tag{6}$$

where the enthalpy is

$$I = [\rho_s\varphi + \rho_l(1-\varphi)](cT - L\varphi) \tag{7}$$

and the heat flux is

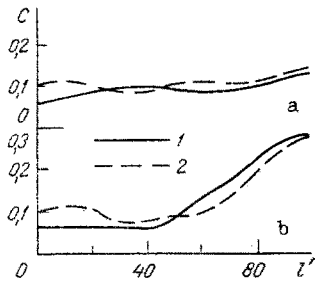

Fig. 3

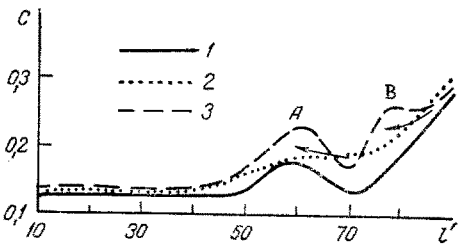

Fig. 4

Fig. 3. Comparison of theoretical (1) and experimental (2) values of the impurity distribution in a horizontal cross section of the ingot: a) at a distance of 10% from the floor; b) 90% from the floor. C, %; ℓ, %.

Fig. 4. Comparison of the experimental (1) and theoretical — with (3) and without (2) taking account of shrinkage — values of the impurity distribution in a vertical cross section of the ingot; ℓ' is the distance from the floor, %.

$$j = -\lambda \nabla T. \tag{8}$$

Combining Eqs. (6)-(8), the following result is obtained, taking account of continuity Eqs. (1)-(3)

$$[\rho_s \varphi + \rho_l (1-\varphi)] \frac{\partial (cT)}{\partial \tau} + \rho_s \nabla (v_{sh} cT\varphi) + \rho_l \nabla [(v_{ly} + v_{lh}) cT (1-\varphi)] =$$
$$= \nabla (\lambda \nabla T) + [L\varphi (\rho_s - \rho_l) + (\rho_s \varphi + \rho_l (1-\varphi)) L] \left(\frac{\partial \varphi}{\partial \tau} + \nabla v_{sh} \varphi \right). \tag{9}$$

In particular, in pouring an ingot into a mold, the velocity of solid-phase motion $v_{sh} = 0$. In the last term on the right-hand side, the component containing $\rho_s - \rho_\ell$ may be omitted. Note the absence of a term with the divergence of $v_{\ell h}$ in determining the source—sink of the heat of crystallization, since the solid phase of the flux is the carrier of this heat.

The initial condition for Eq. (9) here is: $T\big|_{\tau=0} = T_0$. At the boundary with the symmetry condition, zero gradient is specified. At the cooled surface, the boundary condition in the case of convectional transfer takes the form

$$-\left(\lambda \frac{\partial T}{\partial n}\right)_{sur} = \alpha_{con} (T_{sur} - T_c).$$

The proportion of solid phase φ depends on the temperature and mean concentration C of impurity in the given volume. According to the quasi-equilibrium model, the relative quantity of solid phase in equilibrium with the liquid at temperature T is determined by the formula [5]

$$\varphi = (C_l^* (T) - C)/(C_l^* (T) - C_s^* (T)),$$

where $C_\ell^*(T)$ and $C_s^*(T)$ for steel are determined, according to the iron—carbon state diagram, from the following dependences

$$C_l^* (T) = -11.0388 + 0.278656 \cdot 10^{-1} T - 0.120163 \cdot 10^{-4} T^2,$$

$$C_s^* (T) = 15.4633 - 0.124528 \cdot 10^{-1} T + 0.216279 \cdot 10^{-5} T^2.$$

The derivation of impurity-transfer equations in the liquid and solid phases is now considered. The total amount of impurity in the local volume is determined by the relation

$$C = \rho_s C_s \varphi + \rho_l (1-\varphi) C_l.$$

The conservation equation for the concentration C is written in the form

$$\frac{dC}{d\tau} = 0; \quad \frac{d(\rho_s C_s \varphi)}{d\tau} + \frac{d(\rho_l C_l (1-\varphi))}{d\tau} = 0.$$

This equation breaks down into two, each of which describes the change in impurity content separately in the liquid and solid phases. It is necessary to introduce the intensity of interphase mass transfer J here. Taking account of diffusional transfer within each of the phases,

$$\frac{d(\rho_s \varphi C_s)}{d\tau} = -\nabla j_s + J, \quad \frac{d(\rho_s (1-\varphi) C_l)}{d\tau} = -\nabla j_l - J,$$

where $j_s = D_l \nabla (\varphi C_s)$; $j_l = D_l \nabla ((1-\varphi) C_l)$.

The source—sink is defined as follows: If melting occurs, that is,

$$\frac{d\varphi}{d\tau} = \frac{\partial \varphi}{\partial \tau} + \nabla (v_{sh} \varphi) < 0,$$

the impurity concentration in the solid phase C_s = const, and material with impurity content C_s passes to the liquid phase. This means that in the absence of interphase diffusion

$$J = \rho_s C_s \left(\frac{\partial \varphi}{\partial \tau} + \nabla (v_{sh} \varphi) \right).$$

If solidification occurs, i.e., $\frac{d\varphi}{d\tau} = \frac{\partial \varphi}{\partial \tau} + \nabla (v_{sh} \varphi) \geqslant 0$, solid phase with an impurity concentration $C_s^*(T)$ must be formed at temperature T, according to the phase diagram. Thus

$$J = \rho_s C_s^* (T) \left(\frac{\partial \varphi}{\partial \tau} + \nabla (v_{sh} \varphi) \right).$$

The equations of impurity mass transfer on taking account of shrinkage may be written in the form

$$\begin{aligned}
&\frac{\partial (\rho_s C_s \varphi)}{\partial \tau} + \nabla (\rho_s v_{sh} \varphi C_s) = \rho_s \nabla (D_s \nabla (\varphi C_s)) + \\
&+ \begin{cases} \rho_s C_s^* (T) \left(\dfrac{\partial \varphi}{\partial \tau} + \nabla (v_{sh} \varphi) \right), & \dfrac{d\varphi}{d\tau} \geqslant 0, \\ \rho_s C_s \left(\dfrac{\partial \varphi}{\partial \tau} + \nabla (v_{sh} \varphi) \right), & \dfrac{d\varphi}{d\tau} < 0, \end{cases} \\
&\frac{\partial (\rho_l C_l (1-\varphi))}{\partial \tau} + \nabla [\rho_l v_{lh} (1-\varphi) C_l] + \nabla [\rho_l v_{sy} (1-\varphi) C_l] = \\
&\qquad = \rho_l \nabla (D_l \nabla (1-\varphi) C_l) - \\
&- \begin{cases} \rho_l C_l^* (T) \left(\dfrac{\partial \varphi}{\partial \tau} + \nabla (v_{sh} \varphi) \right), & \dfrac{d\varphi}{d\tau} \geqslant 0, \\ \rho_s C_s \left(\dfrac{\partial \varphi}{\partial \tau} + \nabla (v_{sh} \varphi) \right), & \dfrac{d\varphi}{d\tau} < 0. \end{cases}
\end{aligned} \tag{10}$$

In particular, on pouring casting in a mold, v_{sh} is zero.

The initial condition for the solution of Eq. (10) takes the form: $C_s|_{\tau=0} = C_{so}$, $C_\ell|_{\tau=0} = C_{\ell o}$. At the boundaries determined by the symmetry and impermeability conditions, zero gradients are specified for the impurities.

The complexity of the differential equations entails the use of numerical methods of solution. The solution of some simplified models, not including shrinkage convection, was described in [1, 4]. The difficulty of solution is due to the strong nonlinearity of the system, the dependence of the source—sink on the temperature, and the complexity of calculating the liquid-phase fluxes on shrinkage.

The calculation region is shown schematically in Fig. 1, where 1 is the mold; 2 is the floor; 3 is the insulating charge. The liquid metal 4 is separated from the solid core 5 by the two-phase zone 6.

Arrows 7 indicate possible directions of maintenance flow in the temperature-shrinkage zone. For the longitudinal cross section of the ingot, the temperature and concentration fields are assumed to depend on the time and two spatial variables.

An analog of the large-particle method is used for numerical modeling [6]. The method is conservative for each additive characteristic of the medium described by the conservation law. In calculating the convective flows, the Level'e

TABLE 1. Comparison of Experimental and Theoretical Data on the Carbon Distribution in the Ingot Cross Section

Distance from floor, %	Experiment		Calculation	
	at axis	at surface	at axis	at surface
10	−29	−50	+30	−30
90	+133	−50	+150	−30

method is used. To calculate the change in the quantities characterizing the cell in the time step, the uncoupling method is used [6].

The algorithm for solution of the system of equations is now considered in more detail. The following calculations are performed within the time interval for each cell of the calculation region (Fig. 2).

1. Equations (3) and (5) are solved. The possible liquid-phase fluxes at the boundary of each cell are determined (using the technique of directed differences). (The shrinkage flux is calculated separately.)

2. Equation (9) is solved. The state of the cell may change on account of thermoconductive transfer, convective transfer (due to natural or induced convection), and also the action of the source—sink, taking account of the maintenance flows in the solidifying zone of the ingot. Determining the change in state of the cell in an the interval of time, the corresponding temperature value at a new moment of time is calculated by solving the nonlinear equation.

3. Equation (10) is solved. The impurity concentration in the liquid and solid phases of the cell changes as a result of phase transition, convection, and diffusion. Determining the change in state of the cell in the time interval, the corresponding value of the concentration in the liquid and solid phases of the local volume is calculated.

The time step is chosen on the basis of the stability requirement.

As an example, numerical schemes are given for the solution of Eq. (10). The transfer on account of heat conduction in the given time interval is calculated from the formula

$$Q_1 = -\Delta y \frac{\lambda_{i-1j}+\lambda_{ij}}{2} \frac{T_{ij}-T_{i-1j}}{\Delta x} - \Delta y \frac{\lambda_{i+1j}+\lambda_{ij}}{2} \frac{T_{ij}-T_{i+1j}}{\Delta x} -$$

$$-\Delta x \frac{\lambda_{ij-1}+\lambda_{ij}}{2} \frac{T_{ij}-T_{ij-1}}{\Delta y} - \Delta x \frac{\lambda_{ij+1}+\lambda_{ij}}{2} \frac{T_{ij}-T_{ij+1}}{\Delta y}.$$

The change in state of the cell on account of the change in density is

$$Q_{41} = \Delta x \Delta y c_{ij} T_{ij} (\rho_{ij}^n - \rho_{ij}),$$

where ρ^n_{ij} is the density, which is calculated at the new moment of time from the formula: $\rho_{ij}^n = \rho_s \varphi_{ij} + \rho_l (1 - \varphi_{ij})$.

The convective transfer corresponding to the shrinkage component of the flux Q_{42} is now calculated; Q_{42m} is calculated for fluxes directed into the cell and Q_{42p} for fluxes directed out of the cell

$$Q_{42m} = \rho_{i-1j} c_{i-1j} T_{i-1j} m_{ij}|_{m_{ij}>0} - \rho_{i+1j} c_{i+1j} T_{i+1j} m_{i+1j}|_{m_{i+1j}\leqslant 0} +$$
$$+ \rho_{ij-1} c_{ij-1} T_{ij-1} n_{ij+1}|_{n_{ij}>0} - \rho_{ij+1} c_{ij+1} T_{ij+1} n_{ij+1}|_{n_{ij+1}\leqslant 0},$$
$$Q_4 = -Q_{41} + Q_{42m} + Q_{42p},$$

where m_{ij}, m_{i+1j}, n_{ij}, n_{ij+1} are the fluxes through the cell boundary corresponding to the shrinkage component

$$m_{ij} = u_{ij}(1 - \varphi_{ij})|_{u_{ij}\leqslant 0} + u_{ij}(1 - \varphi_{i-1j})|_{u_{ij}>0},$$

and u_{ij} is the shrinkage rate of liquid-phase motion at the cell boundary.

The convective transfer corresponding to the liquid phase is calculated analogously (Q_{2m} is calculated for fluxes directed into the cell and Q_{2p} for those directed out of the cell).

The enthalpy of the cell is

$$Q = \rho_{ij} c_{ij} T_{ij} \Delta x \Delta y + (Q_1 + Q_{2m} + Q_4) \Delta \tau.$$

Solving the nonlinear equation (by the secant method, since the first derivative of the source—sink is not determined at the solidus and liquidus points)

$$Q = [\rho_{ij} C_{ij} T_{ij}^n - \rho_{ij} L \varphi_{ij}^n (T_{ij}^n, C)] \Delta x \Delta y - Q_{2p} T_{ij}^n,$$

hence it is possible to determine: T_{ij}^{n}, $\varphi_{ij}^{n}(T_{ij}^{n}, C)$.

The model developed here is used to study the segregation of carbon with an average carbon content of 0.12%. In the modeling, the fluxes due to thermal convection and mixing in the liquid phase are neglected. In Fig. 3, theoretical and experimental data on the horizontal segregation in casting are presented. Comparison of the carbon concentrations obtained shows that the carbon content increases from the surface to the middle of the ingot and agrees with [4].

A comparison of the deviation of the absolute concentrations of the elements (%) obtained from experiment [4] and as a result of modeling is shown in Table 1.

Theoretical and experimental curves of the axial vertical segregation are shown in Fig. 4. As is evident, the central zone of the ingot has an increased impurity content over the whole axis.

In modeling the solidification process, vertical nonuniformity of the solidification front of periodic character is obtained in the numerical model. The zones of advanced solidification lie at a distance of 40 cm (Fig. 4). This indicates a possibility of describing this phenomenon as the formation of a "bridge" at the base of the model developed. The presence of the bridge means that an isolated volume is formed beneath it. In numerical modeling, maintenance flows to the solidifying volumes occur in the two zones A and B. The direction of these flows is shown by the arrows.

Graphs of the axial segregation of carbon in solidification when the maintenance flows are taken into account and ignored (using equal densities of the liquid and solid phases) are shown in Fig. 4. As is evident, taking account of melt filtration leads to change in the nonuniformity of the carbon content in the axial zone of the ingot by 20% with respect to the mean level.

Note that the model gives an overestimate of the level of axial liquation. In our view, this is due to the use of a quasi-equilibrium model of solidification, which takes no account of the kinetics of nucleation and the crystal growth of the axial zone of the ingot.

As shown above, the model allows the nonuniform vertical solidification of an ingot — i.e., the formation of "bridges" and zones with peak concentrations of carbon at the ingot axis — to be reproduced.

NOTATION

C_s, concentration in the solid phase; C_ℓ, concentration in the liquid phase; C, impurity concentration; φ, proportion of solid phase; v_{sh}, velocity of solid-phase motion; $v_{\ell h}$, velocity of liquid-phase motion; $v_{\ell y}$, shrinkage velocity component; ρ, density; c, specific heat; λ, thermal conductivity; L, specific heat of fusion; D_s, diffusion coefficient in the solid phase; D_ℓ, diffusion coefficient in liquid phase; τ, time interval; α_{con}, coefficient of convective transfer; T, temperature.

LITERATURE CITED

1. M. C. Flemings and G. E. Nereo, Trans. AIME, 242, No. 1, 50-55 (1968).
2. L. Shmrga, Solidification and Crystallization of Steel Ingots [Russian translation], Moscow (1985).
3. H. Nomura, Y. Tarutani, and K. Mori, Trans. ISIJ, 22, 269-276 (1982).
4. A. M. Poyarkov, Steel Production [in Russian], Khar'kov (1955).
5. Yu. A. Samoilovich (ed.), Thermal Processes in the Continuous Casting of Steel [in Russian], Moscow (1982).
6. O. M. Belotserkovskii and Yu. M. Davydov, Large-Particle Method in Gas Dynamics [in Russian], Moscow (1982).